

Comparison of Efavirenz and Dolutegravir on Gut Microbiome and Gut Barrier Functions

Yong-Xiang Huang,[#] Qin Tang,[#] Shi-Hua Fu, Hui-Jun Zhong, Zhe Liu, Qing-Yang Zhong, Yan-Hao Wang, Yin-di Luo, Xue-Ying Li, Song Chen,^{*} and Hai-Peng Zhu^{*}



Cite This: *ACS Omega* 2025, 10, 23099–23110



Read Online

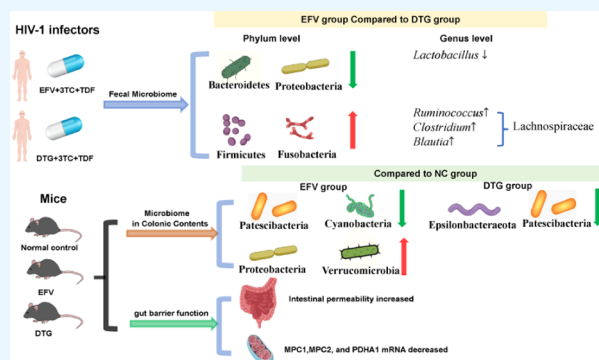
ACCESS |

Metrics & More

Article Recommendations

Supporting Information

ABSTRACT: Dolutegravir (DTG) is increasingly replacing efavirenz (EFV) as the recommended first-line antiretroviral therapy (cART) component due to its superior tolerance. However, both EFV-based and DTG-based cART regimens are associated with metabolic and neuropsychiatric disorders through mechanisms that remain poorly understood. In this study, the abundance of *Lactobacillus* was significantly reduced, along with elevated soluble CD14 levels, in HIV-1-infected individuals receiving EFV-based cART compared to those on DTG-based cART. Additionally, EFV treatment in mice resulted in the destruction of intestinal crypts, loss of goblet cells, decreased expression of intestinal ZO-1, and more severe damage to gut barrier integrity compared to the DTG and normal control groups. Furthermore, we identified a significant reduction in *Lactobacillus* in EFV-treated mice. Our results suggest that EFV and DTG may directly lead to gut dysbiosis and compromised gut barrier integrity, which could be targeted to prevent the side effects associated with EFV and DTG.



INTRODUCTION

Efavirenz (EFV) is a non-nucleoside reverse transcriptase inhibitor (NNRTI) that was recommended as the preferred first-line antiretroviral therapy (ART) in combination with tenofovir disoproxil fumarate (TDF) and emtricitabine (FTC) or lamivudine (3TC) for the treatment of HIV-1, according to the 2013 WHO guidelines. However, EFV has been associated with a high prevalence of neurocognitive disorders among asymptomatic patients. Neuropsychiatric side effects, including vivid dreams, dizziness, insomnia, decreased concentration, anxiety, and depression, could be observed in over 50% of the patients treated with EFV.¹ Additionally, EFV can lead to abnormal lipid metabolism, resulting in a high prevalence of high cholesterol and high-density lipoprotein levels, as well as notable limb fat loss.² Disturbed lipid metabolism may contribute to the pathogenesis of EFV-associated neurocognitive disorders, as EFV treatment led to region-specific lipid alterations in the brains of mice.^{3,4} Consequently, dolutegravir (DTG), a potent and well-tolerated integrase inhibitor, replaced EFV in the 2018 WHO guidelines.⁵ Nevertheless, due to its high antiviral effect, low pill burden, and probably better outcome in T-cell recovery than that of DTG,⁶ EFV continues to be widely used worldwide and administered to millions of patients. Therefore, it is essential to investigate the pathogenesis of EFV-associated adverse effects.

It is well recognized that the gut microbiota exerts profound effects on neuropsychiatric diseases, including autism, mood

disorders, depression,⁷ schizophrenia,⁸ Parkinson's disease⁹ and Alzheimer's disease.¹⁰ Furthermore, mounting evidence has demonstrated the crucial regulatory role of intestinal microbial communities in maintaining energy homeostasis.¹¹ Therefore, we hypothesize that gut dysbiosis mediates the side effects associated with EFV. This hypothesis is supported by the upregulation of NF- κ B, IL-1 β , and TNF- α levels in EFV-administered cases.¹² To investigate this, we compared the effects of EFV- and DTG-based cART regimens on the gut microbiota in HIV-1-infected individuals. Additionally, we examined the impacts of EFV and DTG on gut microbiota in mice to further validate their effects.

RESULTS

Clinical Characteristics. The clinical characteristics of all the enrolled patients are presented in [Table 1](#). There is no significant difference in age between the EFV and DTG groups. The viral load of all HIV-infected individuals receiving cART is undetectable (<40 copies/mL) for more than 6 months. The baseline and most recent CD4+T cell counts are

Received: February 8, 2025

Revised: May 14, 2025

Accepted: May 22, 2025

Published: May 30, 2025



Table 1. Clinical Characteristics of Enrolled HIV-1 Infectors^a

Clinical characteristics	DTG-based cART (male, N = 7)	EFV-based cART (male, N = 10)	p-value
Age, median (95% CI)	40.0 (31.7–52.0)	33.0 (31.0–43.4)	0.417
HIV viral load (cp/ml)	all <40	all <40	1.000
Last CD4+ counts (cells/mm ³), median (95% CI)	425.0 (203.9–815.5)	593.0 (390.8–795.2)	0.475
Baseline CD4 counts (cells/mm ³), median (95% CI)	105.0 (–1.9–421.9)	368.5 (212.9–482.1)	0.161
cART duration (months), median (95% CI)	51.4 (33.1–81.9)	53.9 (38.2–85.6)	1.000
Switched to DTG (months), median (95% CI)	18.0 (9.6–32.1)	/	
Lipid panel			
TC (mmol/L), mean ± SD	4.47 ± 0.54	4.69 ± 1.16	0.660
TG (mmol/L), mean ± SD	1.75 ± 1.21	2.12 ± 1.07	0.527
HDL-c (mmol/L), mean ± SD	1.17 ± 0.21	1.19 ± 0.31	0.887
LDL-c (mmol/L), mean ± SD	2.82 ± 0.58	2.98 ± 0.85	0.670
Bacterial translocation			
LPS (pg/mL), mean ± SD	78.9 ± 33.3	78.8 ± 45.6	0.997
sCD14(ng/mg), mean ± SD	787.9 ± 392.6	1346.0 ± 493.7	0.025
T cell activation			
DR+CD38+ in CD4, mean ± SD	9.1% ± 4.3%	7.7% ± 4.1%	0.613
DR+CD38+ in CD8, mean ± SD	32.7% ± 10.5%	26.6% ± 13.9%	0.450

^aCI: confidence interval; TC: total cholesterol; TG: triglycerides; HDL-c: high-density lipoprotein cholesterol; LDL-c: low-density lipoprotein cholesterol.

slightly lower in DTG recipients compared to the EFV group, with this trend remaining nonsignificant. The duration of cART showed no significant variation when comparing the EFV and DTG groups.

Then, we compared the blood levels of a lipid panel, which included total cholesterol (TC), triglycerides (TG), low-density lipoprotein cholesterol (LDL-c), and high-density lipoprotein cholesterol (HDL-c). The average levels of TC, HDL-c, and LDL-c in both groups were within the normal range, while the average TG levels (1.75 ± 1.21 and 2.12 ± 1.07 mmol/L in the DTG and EFV groups, respectively) exceeded the normal range (0.56–1.70 mmol/L). All four parameters in the EFV group were higher than those in the DTG group, although the differences were not statistically significant.

Additionally, we measured the blood levels of lipopolysaccharide (LPS) and soluble CD14 (sCD14) to assess gut bacterial translocation. sCD14 levels in the EFV group were significantly higher than those in the DTG group ($p < 0.05$), whereas the LPS levels were comparable between the two groups. With the combined surface staining of HLA-DR and CD38, we identified activated CD4 and CD8 T cell populations. The proportions of activated CD4 and CD8 cells were similar between the EFV and DTG groups.

Comparison Between EFV and DTG on Fecal Bacterial Microbiome. The 16S rDNA sequencing of 17 fecal samples generated 2,038,073 high-quality reads with an average length of 418 bp, which were subsequently assembled into 1,156,715 tags, averaging 68,042 tags per sample. Further, rarefaction and Shannon curves were plotted to estimate species richness as indices of sequencing depth at the taxonomic levels (Figure S1A,B). Both rarefaction and Shannon curves reached stable plateaus, indicating appropriate sampling completeness. A rank-abundance distribution curve for the microbial communities was constructed to visualize species richness and species evenness, which implied similar species richness and evenness in the EFV and DTG groups (Figure S1C). Species accumulation curves (Specaccum) were also plotted to compare the diversity properties of community data sets (Figure S1D).

Compared to the DTG group, the EFV group exhibited a lower abundance of Bacteroidetes and Proteobacteria, while showing a higher abundance of Firmicutes and Fusobacteria at the phylum level (Figure 1A). To evaluate intergroup variations in microbial community composition, we calculated alpha diversity indices as ecological metrics. As shown in Figure 1B–E, the Chao1, Simpson, Shannon, and Observed species indices in the EFV group were slightly higher than those in the DTG group; however, the observed differences did not reach statistical significance ($p > 0.05$). To illustrate differences in OTU composition among samples, we employed principal coordinates analysis (PCoA) with Weighted UniFrac analysis to create a 2D ordination plot representing major compositional gradients. The first coordinate (PCoA 1) accounted for 56.6% of the intersample variance, while PCoA 2 accounted for 16.6% of the differences among the three groups (Figure 1F). The EFV group could not be distinctly separated from the DTG group.

With LEfSe analysis, the primary differences between the EFV and DTG groups at various taxonomy levels are the loss of the *Lactobacillus* genus and the enrichment of three genera (*Ruminococcus*, *Clostridium*, and *Blautia*) from the *Lachnospiraceae* family (Figure 1G). KEGG pathway analysis revealed functional profiles comparable to those of the EFV and DTG groups (Figure 1H).

EFV and DTG Treatments Resulted in Gut Barrier Damage in Mice. Then, we aimed to recapitulate the gut dysbiosis and bacterial translocation induced by EFV in mice. Across the experimental timeline, the weight parameters of the entire animal cohort gradually increased, except for a temporary decrease in EFV-treated mice during the first week. Furthermore, mice receiving EFV treatment gained significantly less weight from week 2 onward, and this trend persisted throughout the experiment (Figure 2A). DTG treatment also resulted in a slight reduction in weight gain, although this was not statistically significant compared to the NC group.

Considering that cART could impair glucose tolerance in HIV-1-infected patients, we conducted a standard oral glucose tolerance test (OGTT) for each animal every 2 weeks.

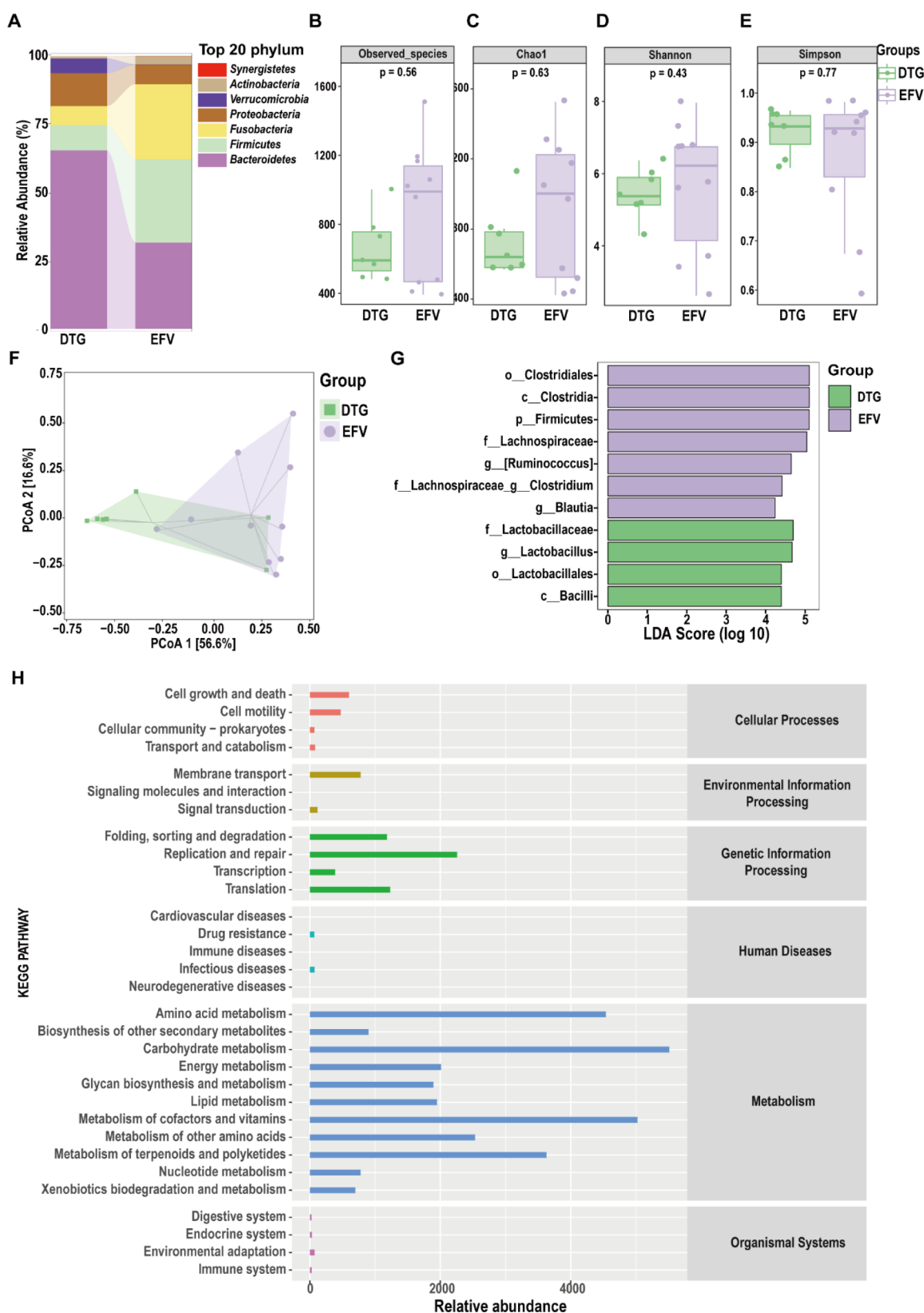


Figure 1. Effects of efavirenz (EFV)-based and dolutegravir (DTG)-based antiretroviral therapy on the gut microbial community. (A) Comparison of bacterial abundance between EFV and DTG groups at the phylum level. (B–E) Alpha diversity indices were employed to assess the microbial community richness and evenness in the EFV and DTG groups. (B) Observed species, (C) Chao1, (D) Shannon, and (E) Simpson indices were presented using box plots. (F) Unweighted UniFrac-based PCoA plot of the bacterial community showed the diversity among groups. Parenthetical numerals indicate the proportion of variance explained by individual principal components across samples. (G) Liner discriminant analysis (LDA) effect size (LEFSe) analysis of the relative bacterial abundance between the EFV and the DTG groups. (H) The predicted KEGG pathways based on the average abundance of the overall bacteria identified in this study.

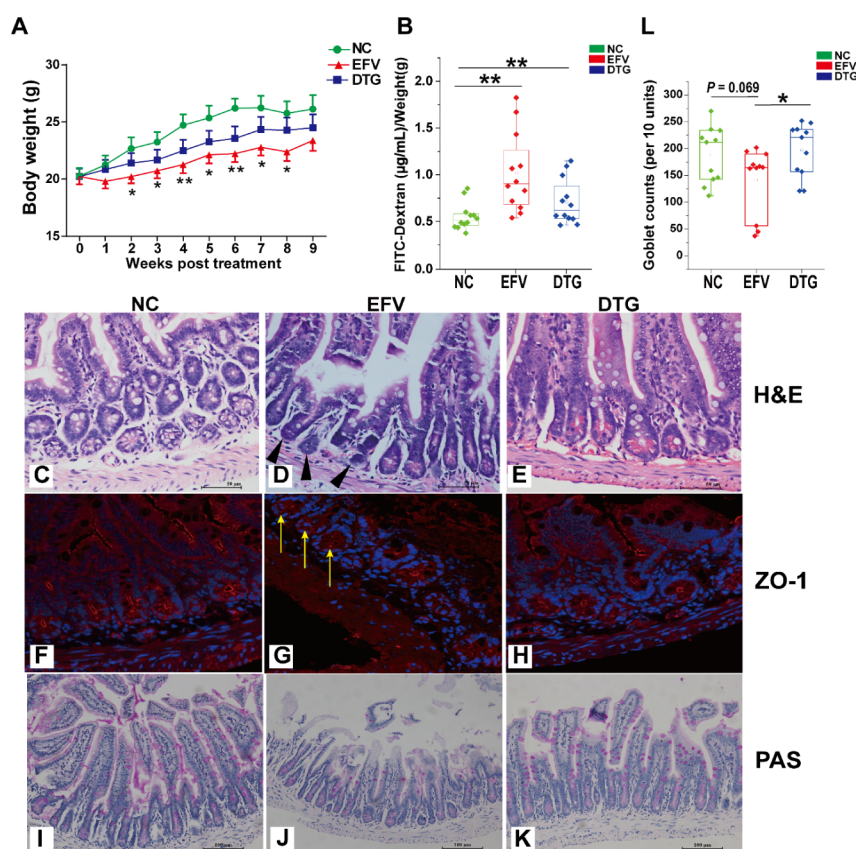


Figure 2. Effects of EFV and DTG on body weight and intestinal barrier function. (A) Dynamics of body weight (mean \pm SD, $N = 12$ for each group). *, **: $p < 0.05$ and $p < 0.01$ compared to the normal control (NC) group, respectively. (B) The plasma levels of FITC-dextran indicating gut permeability 1 h after oral FITC-dextran administration. Values were normalized to body weight. Data are presented as mean \pm SD values. $N = 12$ for each group. **: $p < 0.01$. (C–E) Representative pictures of ileal histopathologic changes in mice with H&E staining. Ileal samples from mice in (C) NC, (D) EFV, and (E) DTG groups were used. (F–H) Representative pictures of immune-fluorescent staining of zona occludens-1 (ZO-1). (F) NC, (G) EFV, and (H) DTG groups. Alexa Fluor 594 (red) and DAPI (blue) were used for ZO-1 and nuclear staining, respectively. (I–K) Representative pictures of ileal Periodic Acid-Schiff (PAS) staining indicating goblet cells, with samples from (I) NC, (J) EFV, and (K) DTG groups. (L) Goblet cell counts are shown in columns. Data are presented as mean \pm SD values. $N = 12$ for each group. *: $p < 0.05$.

However, as shown in Figure S2A the fasting glucose levels were not affected by either EFV or DTG treatments throughout the experiment. In contrast, EFV caused a significant decrease in peak glucose level at 15 min after intragastric glucose injection compared to the NC group. This alteration emerged early (at 2 weeks) and was maintained throughout the experiment, resulting in a significantly lower area under Curve (AUC) of the OGTT in the EFV group compared to the NC group at weeks 6 and 8 (Supporting Information, Figure S2AB). Furthermore, histological examination revealed lipotrophy and lymphocyte infiltration in white adipose tissue (Figure 3A–C) and hepatolysis in the liver (Figure 3D–F) in EFV-treated mice. These abnormalities imply that we have recapitulated the commonly reported adverse effects of EFV.

We further compared the effects of EFV versus DTG on gut barrier function, as indicated by the FITC-dextran assay. As shown in Figure 2B, both EFV and DTG treatments resulted in a significant increase in plasma FITC-dextran concentration (both $p < 0.01$ compared to the NC group), indicating increased gut barrier permeability. Comparative analysis indicated marginally higher but statistically insignificant FITC-dextran values in the EFV versus DTG treatment arms.

Furthermore, H&E staining revealed that EFV treatment significantly disrupted the crypt structure, leading to crypt

atrophy and even crypt loss (indicated by the short arrow in Figure 2C–E). Additionally, immunofluorescence staining of intestinal tight-junction molecules, ZO-1, showed weakened staining in the crypts of mice receiving EFV treatment (indicated by the long arrow in Figure 2F–H). Moreover, EFV treatment resulted in a substantial loss of goblet cells compared to the DTG treatment and a marginally significant loss compared to the NC group, with representative images displayed in Figure 2I–K. The corresponding goblet cell counts are presented in columns (Figure 2L).

The underlying mechanisms by which efavirenz (EFV) and dolutegravir (DTG) impair gut barrier function remain unclear. Previous studies have reported mitochondrial toxicity associated with EFV and DTG.^{13,14} Consequently, we examined the expression profiles of genes encoding enzymes involved in pyruvate metabolism, including mitochondrial pyruvate carriers MPC1 and MPC2, as well as pyruvate dehydrogenase (PDHA1). Additionally, we assessed the subunits of mitochondrial complex I (NADH:ubiquinone oxidoreductase), specifically NDUFV1, NDUFV2, and NDUF51, along with complex II (SDHA) of the mitochondrial respiratory chain. We also included glyceraldehyde 3-phosphate dehydrogenase (GAPDH), which catalyzes the sixth step of glycolysis. As shown in Figure S4, DTG significantly inhibited the mRNA expression of MPC1,

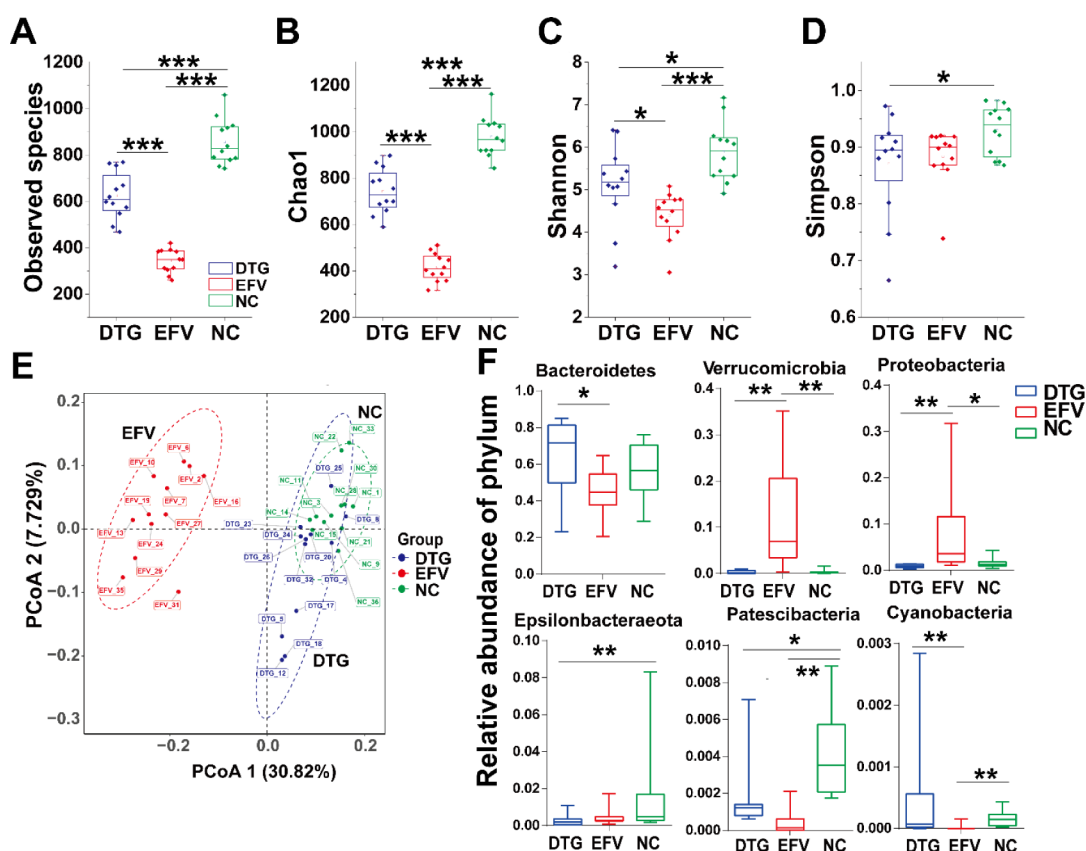


Figure 3. Effects of dolutegravir (DTG) and efavirenz (EFV) on the gut microbial community distribution in mice. (A) Dynamics of body weight (mean \pm SD, $N = 12$ for each group). *, **: $p < 0.05$ and $p < 0.01$ compared to the normal control (NC) group, respectively. (B) The plasma levels of FITC-dextran indicating gut permeability 1 h after oral FITC-dextran administration. Values were normalized to body weight. Data are presented as mean \pm SD values. $N = 12$ for each group. **: $p < 0.01$. (C–E) Representative pictures of ileal histopathologic changes in mice with H&E staining. Ileal samples from mice in (C) NC, (D) EFV, and (E) DTG groups were used. (F–H) Representative pictures of immunofluorescent staining of zona occludens-1 (ZO-1). (F) NC, (G) EFV, and (H) DTG groups. Alexa Fluor 594 (red) and DAPI (blue) were used for ZO-1 and nuclear staining, respectively. (I–K) Representative pictures of ileal Periodic Acid-Schiff (PAS) staining indicating goblet cells, with samples from (I) NC, (J) EFV, and (K) DTG groups. (L) Goblet cell counts are shown in columns. Data are presented as mean \pm SD values. $N = 12$ for each group. *: $p < 0.05$.

MPC2, and PDHA1. EFV also significantly reduced PDHA1 and NDUFV1 expression, while NDUFS1 and SDHA were not significantly affected by either DTG or EFV.

Comparison of EFV and DTG on the Microbiota Community in the Colonic Contents of Mice. A total of 3,073,233 high-quality reads, with an average length of 422 bp, were obtained from 36 colonic content samples. These reads were combined into 1,375,668 tags, resulting in an average of 38,213 tags per sample. We further plotted the Rarefaction and Shannon curves to estimate species richness as indices of sequencing depth at the taxonomic levels. As shown in Figure SSA,B, both diversity curves (rarefaction and Shannon) approached saturation, suggesting adequate sequencing coverage. To evaluate community structure, we plotted rank-abundance distributions depicting both richness and evenness, revealing that EFV apparently caused a significant reduction in species richness (Figure SSC). Species accumulation curves (Specaccum) were also plotted to compare the diversity properties of the data sets (Figure SSD).

To assess the overall differences in microbial community structure among the groups, we measured ecological parameters based on alpha diversity, including Observed Species, Chao1, Simpson, and Shannon indices. As shown in Figure 3A–D, the Observed Species, Chao1, and Shannon

indices significantly decreased in the DTG group compared to the NC group ($p < 0.001$ for Observed Species and Chao1 indices, and $p < 0.05$ for the Shannon index). The decrease in the EFV group was even more pronounced for all of these indices. While DTG administration led to significantly diminished Simpson index scores relative to NC ($p < 0.05$), EFV treatment preserved normal diversity levels. To illustrate the differences in OTU composition among the various samples, a PCoA with Weighted UniFrac analysis was performed. The PCoA plot revealed a distinct clustering separation of the different groups, with the EFV group clearly separated from the partially overlapping NC and DTG groups, indicating a more severe impact of EFV than DTG (Figure 3E).

According to the phylum-level annotations of the operational taxonomic units (OTUs), we compared the relative abundances of the ten most enriched phyla: Bacteroidetes, Firmicutes, Verrucomicrobia, Proteobacteria, Epsilonbacteraeota, Actinobacteria, Patescibacteria, Fusobacteria, Tenericutes, and Cyanobacteria. These were analyzed using the Kruskal–Wallis test. Compared to the NC group, Epsilonbacteraeota and Patescibacteria showed a significant decrease in the DTG group ($p < 0.01$ and $p < 0.05$, respectively). In contrast, Verrucomicrobia and Proteobacteria exhibited

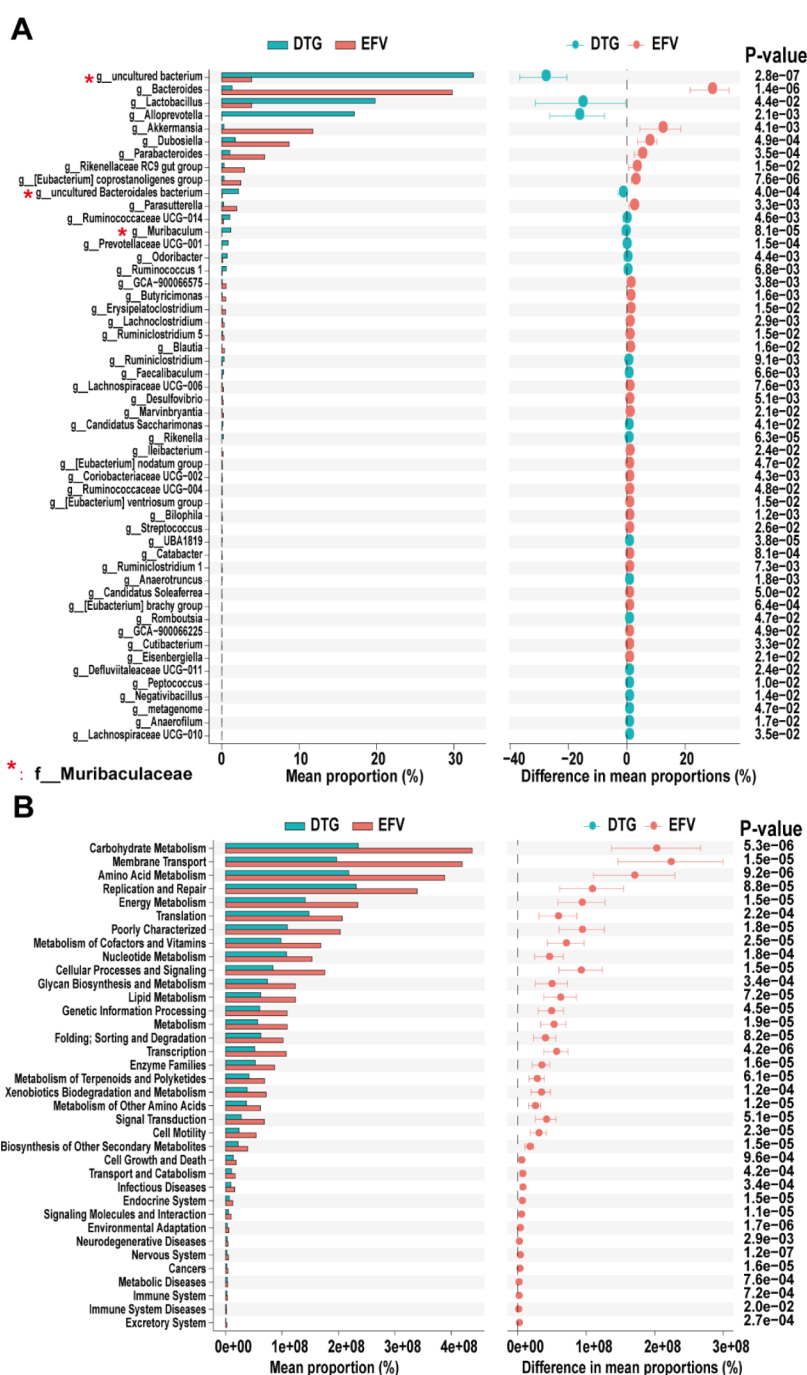


Figure 4. Genera with differential abundance and predicted Kyoto Encyclopedia of Genes and Genomes (KEGG) pathways enriched in comparison with EFV and DTG groups in mice.

significant increases ($p < 0.01$ and $p < 0.05$, respectively), along with a notable decrease in the abundances of Patescibacteria and Cyanobacteria (both $p < 0.01$) in the EFV group (Figure 3F).

We further compared the effects of EFV and DTG on the gut microbiota in mice. As shown in Figure 4A, a total of 52 bacterial genera were identified with significantly different abundances using a threshold of $p < 0.05$ (STAMP, t -test). Ranked by the difference in mean proportions, the top five genera that exhibited remarkable changes in the EFV group were decreased “uncultured bacterium” (belonging to the Muribaculaceae family), *Alloprevotella*, and *Lactobacillus*, while *Bacteroides* and *Akkermansia* showed an increase. The top five

enriched KEGG pathways in the EFV group were “Carbohydrate Metabolism”, “Membrane Transport”, “Amino Acid Metabolism”, “Replication and repair”, and “Energy Metabolism” (Figure 4B).

(A) Relative proportion of genera with differential abundance in the comparison between EFV and DTG groups (STAMP, t -test). (B) Predicted KEGG pathways with differential relative proportions in the comparison between the EFV and DTG groups.

EFV caused a significant alteration in gut microbiota compared to that of the NC group. At the genus level, a total of 75 bacterial taxa exhibited significantly different abundances ($p < 0.05$) as determined by STAMP t -tests, with a

threshold of $p < 0.05$. The top five bacterial genera that showed the most notable changes included a decrease in “uncultured bacterium” (belonging to the *Muribaculaceae* family) and *Lactobacillus*, alongside an increase in *Bacteroides*, *Akkermansia*, and *Dubosiella*. The top five enriched KEGG pathways were similar to those identified in the comparison between the EFV and DTG groups (Figure S6).

In contrast, mice receiving DTG treatment exhibited less gut dysbiosis compared with those in the NC group. When ranked by the difference in mean proportions, the five most enriched genera included a decrease in “other” (belonging to the *Lachnospiraceae* family), “uncultured Bacteroidales bacterium” (belonging to the *Muribaculaceae* family), and *Lachnospiraceae* NK4A136 group, while *Alloprevotella* and *Alistipes* showed an increase (Figure S7A). Based on PICRUSt analysis, a total of four differential KEGG pathways were identified. These included an increase in the “Digestive System” pathway and a decrease in the “Cell Motility”, “Cell Communication”, and “Sensory System” pathways (Figure S7B).

DISCUSSION

Understanding the pathogenesis of cART-associated side effects is crucial for improving the clinical efficacy and safety of long-term cART administration. While EFV is associated with hepatotoxicity, neurotoxicity, and cardiovascular adverse events, its mechanisms remain poorly understood. Interestingly, microbial translocation has been implicated in liver disease, cardiovascular disease, and neurocognitive disorders in HIV-1 infection.¹⁵ Therefore, we speculate that EFV may exacerbate microbial translocation, trigger chronic inflammation, and consequently contribute to EFV-associated side effects. In this study, we observed significantly higher blood FITC-dextran levels in EFV-treated mice compared with the DTG group, suggesting increased gut microbial translocation into systemic circulation. The higher sCD14 levels observed in HIV-1-infected individuals receiving EFV-based cART than in patients in the DTG group also implied more severe bacterial translocation, supporting our hypothesis.

The intestinal barrier integrity plays a crucial role in restricting bacterial translocation. The association between intestinal barrier integrity and neuropsychiatric side effects has been well documented.¹⁶ In this study, we demonstrated that EFV treatment reduced ZO-1 expression and induced goblet cell loss, providing direct evidence of impaired gut barrier integrity.

There exists intricate crosstalk between gut microbes and the intestinal barrier, which comprises mechanical, microbial, chemical, and immune barrier components. As a representative example, short-chain fatty acids (SCFAs), microbial-derived metabolites, are indispensable both for enterocyte energy provision and for maintaining redox balance and microbiota homeostasis. Consequently, dysbiotic microbiota can drastically compromise the gut barrier. Notably, certain cART drugs could directly inhibit the growth of bacteria *in vitro*. As an example, EFV has been shown to inhibit the growth of *Enterococcus*, *Bacteroides*, and *Prevotella* *in vitro*.¹⁷ Zidovudine and EFV also shape the gut microbiome *in vivo*.¹⁷ In this study, we compared the impacts of DTG-based and EFV-based cART on gut microbiota in HIV-1-infected individuals. The typical changes observed in the EFV group included a decrease in *Lactobacillus* and an increase in several members of “*Lachnospiraceae* family” compared to the DTG group. Consistently, we also noted a loss of *Lactobacillus* in EFV-

treated mice. *Lactobacillus* has long been associated with maintaining gut barrier integrity.¹⁸ These findings provide us with a novel perspective for understanding the pathogenesis of the adverse effects associated with EFV. The differences in microbial alterations between our study and previous reports could probably be due to factors such as race, region, and diet.

Besides gut dysbiosis, the impairment of gut barrier integrity following treatment with EFV or DTG may also be attributed to disrupted mitochondrial functions. It is well established that mitochondrial toxicity plays a key role in the side effects associated with EFV and DTG.^{19,20} EFV specifically inhibits complex I,¹⁴ while DTG inhibits complex IV.^{20,21} Mitochondrial bioenergetics are crucial for the repair of intestinal barriers during simian immunodeficiency virus (SIV) infection.²² Furthermore, pyruvate is necessary and sufficient to sustain the proliferation of intestinal stem cells.²³ Pyruvate is transferred into the inner mitochondrial matrix by MPC1 and MPC2,²⁴ converted into acetyl-CoA by the pyruvate dehydrogenase complex, and subsequently subjected to the TCA cycle for oxidative phosphorylation. In this study, we observed that EFV significantly inhibited the intestinal expression of PDHA1 and NDUFV1 (encoding the 51 kDa subunit of complex I), while DTG downregulated MPC1, MPC2, and PDHA1 expressions. These findings suggest that DTG and EFV differentially disrupt pyruvate metabolism and mitochondrial complex functions, which could theoretically impair the gut barrier's integrity.

We also noted differences in the dysbiosis caused by EFV between humans and mice. First, EFV led to a significant loss of alpha diversity in mice but not in HIV-1-infected individuals. The richness of the human gut microbiome correlates with various metabolic markers.²⁵ This discrepancy suggests that EFV treatment resulted in more severe gut dysbiosis and metabolic disorders in mice compared to those in humans. Furthermore, we observed a remarkable loss of members of the *Muribaculaceae* family in EFV-treated mice, while no such loss was observed in HIV-1-infected individuals. *Muribaculaceae* family exhibits a cross-feeding relationship with *Lactobacillus*, and its enrichment has been associated with obesity and diabetes.²⁶ These differences may be attributed to the species variation between humans and mice. However, we maintain that EFV-treated healthy mice are still valuable animal models for investigating EFV-associated side effects. In this study, we replicated the common side effects of EFV, including histopathologic abnormalities in white adipose and liver tissues. Notably, the temporary decrease in body weight in EFV-treated mice during the first week could also be explained with the psychiatric side effects of EFV, which begin quickly and commonly peak in the first 2 weeks.²⁷

Unexpectedly, our research revealed that the gut barrier integrity was also compromised in mice receiving the DTG treatment. Compared to the NC group, the most notable alteration in the DTG-treated mice was the loss of *Lachnospiraceae* NK4A136. *Lachnospiraceae* NK4A136, known for producing short-chain fatty acids (SCFAs), is typically associated with maintaining intestinal barrier integrity in mice.²⁸ The loss of *Lachnospiraceae* NK4A136 has also been linked to autism spectrum disorder,²⁹ anxiety, and depression.³⁰ Therefore, our findings provide an explanation for the neuropsychiatric side effects associated with DTG treatment.

This investigation presents two primary limitations that warrant further examination in subsequent studies. First, while we postulated that gut dysbiosis and bacterial translocation

might contribute to EFV-associated side effects, cognitive functions were not assessed in either human subjects or murine models. Neuropsychiatric effects are the most concerning side effects of EFV. As brain microbial populations in HIV/AIDS have been identified,³¹ whether EFV aggravates brain microbial invasion through EFV-associated gut leakage would be a very interesting question. Second, this study did not include metabolomic analyses. As we mentioned above, gut microbiota help maintain intestinal barrier functions partially through their metabolites, like SCFAs. The fecal metabolomics analysis would significantly contribute to understanding the mechanistic relationship between EFV/DTG-associated gut dysbiosis and compromised barrier functions. Further experimental investigations are needed to address these scientific questions.

CONCLUSION

Both DTG and EFV caused gut dysbiosis and impaired gut barrier function. Targeting the gut microbiota might be a potential therapeutic strategy for metabolic and neuropsychiatric disorders associated with cART.

METHODS

Patients. A total of 17 follow-up cases who received free cART at Dongguan Ninth People's Hospital from September to November 2023, including 7 individuals receiving a DTG-based regimen (DTG, 3TC, and TDF) and 10 individuals receiving an EFV-based regimen (EFV, 3TC, and TDF), were enrolled. The dose of EFV was 400 mg/day. All cases were males aged 28–56 years, and their plasma viral load remained below detectable levels (less than 40 copies/mL) for more than 6 months. All enrolled patients in the DTG group had received the DTG-based cART regime for more than 1 year. None of the cases had a history of diabetes or cancer and did not take antibiotics or other drugs that might affect the intestinal flora.

Ethics Statement. Individuals enrolled in the research provided written informed consent, authorizing the utilization of data collected during their standard clinical care for research purposes. The research protocol received approval from the Medical Research Council of Dongguan People's Hospital (No.AF-97–02). The study data were stored in a password-protected electronic medical records system and were accessed only by authorized clinic personnel. These anonymized records were provided to the statistical analysis team in a deidentified format that prevented individual identification.

Fecal Sample Collection and DNA Extraction. During scheduled clinic visits, participants' fecal samples were aseptically collected in sterile containers and cryopreserved at $-80\text{ }^{\circ}\text{C}$. Genomic DNA was extracted according to the manufacturer's protocols³² using the QIAamp DNA Stool Mini Kit (QIAGEN, Hilden, Germany), coupled with mechanical lysis via a Mini-Bead Beater (FastPrep; Thermo Electron Corporation, Boston, MA, USA). Nucleic acid purity and concentration were determined spectrophotometrically (NanoDrop 1000, Thermo Electron Corporation, USA), with subsequent evaluation of molecular integrity through 1.2% agarose gel electrophoresis.

16S rRNA Sequencing. The full-length 16S rRNA sequencing workflow, including amplification, cloning, and sequencing, was implemented at Repugene Technology Co., Ltd. (Hangzhou, China). PCR amplification was conducted using universal primers targeting 16S V3–V4 (341F-806R),

which incorporated unique sample barcode systems for sample sequences.³³ PCR amplification was performed in 50 μL reactions containing 20 ng genomic DNA sample, 1.25 U Taq DNA polymerase, 5 μL 10 \times Ex Taq buffer, 10 mM dNTPs (all reagents from TaKaRa Biotechnology Co., Ltd., Dalian, China), and 40 pmol primer mix. Thermal cycling conditions included 5 min of initial denaturation at $95\text{ }^{\circ}\text{C}$; 28 cycles of $95\text{ }^{\circ}\text{C}$ for 30 s (denaturation), $55\text{ }^{\circ}\text{C}$ for 30 s (annealing), and $72\text{ }^{\circ}\text{C}$ for 45 s (elongation), followed by a final extension at $72\text{ }^{\circ}\text{C}$ for 7 min. Amplification products were mixed 1:1 with SYBR Green-containing loading buffer, and electrophoresis was performed on a 2% agarose gel. Target amplicons (400–450 bp) exhibiting distinct electrophoretic profiles were excised for subsequent analysis. Postamplification, DNA fragments were purified using the AxyPrep DNA Gel Extraction Kit (AXYGEN Biosciences, Union City, CA, USA); sequencing libraries were prepared with the NEB Next Ultra DNA Library Prep Kit (Illumina, NEB, USA) per manufacturer protocols, with index codes. The library quality control comprised fluorometric quantification (Qubit@ 2.0 Fluorometer, Thermo Scientific) and electrophoretic analysis (Agilent Bioanalyzer 2100). Finally, sequencing of the library on the Illumina MiSeq/Novaseq 6000 platform was performed, and paired-end reads were deposited in the Sequence Read Archive (SRA) under accession numbers PRJNA1196606 (clinical samples) and PRJNA900705 (samples from mice).

For bioinformatics analysis, paired-end reads from the original DNA fragments were processed by using FLASH, a highly efficient and precise analysis tool. FLASH is designed to merge paired-end reads when at least partial overlap exists between forward and reverse reads generated from the same DNA fragment. Sample-specific paired-end reads were sorted based on unique barcode identifiers.

The analysis of sequences was conducted by using the UPARSE software package with the UPARSE-OTU and UPARSE-OTUref algorithms. Custom Perl scripts were employed to evaluate alpha (within-sample) and beta (among-sample) diversity. Sequences sharing $\geq 97\%$ sequence similarity were clustered into identical operational taxonomic units (OTUs). A representative sequence was selected for each OTU, and taxonomic annotation was assigned using the RDP classifier for each representative sequence. To compute Alpha Diversity, the OTU table was rarefied to standardized sequencing depth, followed by calculation of three ecological metrics: The observed Species, which estimates the number of unique OTUs found in each sample; the Chao1, which estimates species abundance; and Shannon and Simpson indices, which estimate biodiversity. Rarefaction curves were generated to evaluate the sampling completeness through these three metrics. Graphical representation of the relative abundance of bacterial diversity across taxonomic ranks (phylum to species) was visualized through the Krona interactive chart. Principal Coordinate Analysis (PCoA) was conducted using unweighted UniFrac distances, aiding in obtaining principal coordinates and visualizing them from high-dimensional data sets.

To confirm differences in the abundances of individual taxa between the two groups, STAMP software was utilized. LDA effect size (LEfSe) was used for the quantitative analysis of biomarkers within different groups and was visualized with a Cladogram. This method was designed to analyze data in which the number of species is much higher than the number of samples and to provide biological class explanations to

establish statistical significance, biological consistency, and effect-size estimation of the predicted biomarkers. Graphical representation of the relative abundance of bacterial diversity from phylum to species can be visualized using a Krona chart. Functional predictions were performed using PICRUSt to annotate Kyoto Encyclopedia of Genes and Genomes (KEGG) Orthology (KOs) and Clusters of Orthologous Groups (COGs).³⁴

Blood Sample Collection and Routine Monitoring of Viral Load and CD4 Counts. Immediately after sample collection, plasma and peripheral blood mononuclear cells (PBMCs) were separated from whole blood and stored at $-80\text{ }^{\circ}\text{C}$ for batch assays. According to a routine monitoring protocol, quantification of HIV-1 RNA load in plasma was conducted using Cobas Amplicor (Roche, USA). CD4+T counts were also quantified with BD Tritest CD4 FITC/CD8 PE/CD3 PerCP (BDIS, USA), and flow cytometry analysis was carried out using CytoFLEX cytometry (Beckman Coulter, China).

T Cell Populations. Flow cytometry analysis of the activated T-cell population was performed using the following fluorescence-labeled monoclonal antibodies: CD3-PerCP (clone SP34.2), CD4-FITC (clone L200), CD38-PE (clone HIT2), and HLA-DR APC (clone G46-6). All antibodies were acquired from BD Biosciences (USA).

Laboratory Assays for Soluble CD14 (sCD14) and Lipopolysaccharide (LPS). In addition, plasma levels of markers for microbial translocation, LPS, and soluble sCD14 were determined using enzyme-linked immunosorbent assay (ELISA) kits purchased from Cusabio Technology LLC (Wuhan, China). All assays were performed following the manufacturer's instructions. Values were read with a Varioskan LUX microplate reader (Thermo Scientific Inc., USA).

Animals. Seven-week-old male C57BL/6J mice were acquired from the Guangdong Medical Laboratory Animal Center (GDMLAC) and maintained in specific pathogen-free (SPF) barrier facilities (temperature $23 \pm 2\text{ }^{\circ}\text{C}$, humidity $60 \pm 10\%$, 12/12 h light–dark cycle).

Animals received purified water and autoclaved standard rodent chow ad libitum. The protocols were ethically reviewed and sanctioned by the Animal Experimental Ethical Committee of the GDMLAC (No. 2018007). Procedures strictly conformed to the NIH Guide for the Care and Use of Laboratory Animals.³⁵

Following a 1-week acclimation period, a total of 36 mice were randomly assigned into three groups, namely, the DTG, EFV, and normal control (NC) groups, with 6 males and 6 females in each group. Animals in the DTG and EFV groups were intragastrically administered with 20.6 mg/kg DTG (equivalent to the adult dose of 100 mg/day) or 123.3 mg/kg EFV (equivalent to 600 mg/day), respectively. DTG and EFV tablets were purchased from Glaxo Operations UK Ltd. or Shanghai Desano Pharmaceuticals Co., Ltd., respectively, and minced and suspended in 0.5% carboxymethyl cellulose sodium (CMC-Na, Tianjin FUCHEN Chemical Reagent Factory, China). Animals in the NC group received equivalent dosing volumes (10 mL/kg) of vehicle control (0.5% CMC-Na solution) through matched administration regimens. All treatments were performed once per day for 60 consecutive days.

For mice, colonic contents were aseptically harvested into a sterilized cryovial, immediately frozen in liquid nitrogen, and maintained at $-80\text{ }^{\circ}\text{C}$ until bacterial DNA extraction and

isolation were conducted utilizing the previously validated protocol.

Fasting Glucose Level and Oral Glucose Tolerance Test (OGTT). Prior to the glucose tolerance test, mice were transferred into a cage with fresh bedding and fasted overnight (16 h) before performing the glucose tolerance test. A glucose load of 2 g/kg of body weight was administered by intragastric gavage, and blood samples were collected from the tail vein at times 0, 15, 30, 60, and 120 min. Blood glucose quantification was obtained using the OneTouch Ultra system (Johnson & Johnson, USA).

Gut Leakage Measurement. Gut permeability was assessed via a fluorescein isothiocyanate-dextran (FITC-dextran) assay. FITC-dextran, a nonabsorbable molecule (3–5 kDa; Sigma-Aldrich, St. Louis, MO, USA), was diluted to 100 mg/mL with PBS and administered to mice by gavage at a dose of 0.6 mg/g once after a 4-h fast on the day after the termination of treatment. After 1 h, blood was collected, anticoagulated, and plasma samples were separated and subjected to FITC-dextran detection immediately. To create a standard curve, unused FITC-dextran (100 mg/mL) was serially diluted with water. The fluorescence intensity values were read in a Varioskan LUX multimode microplate reader (ThermoFisher, USA) with 485 nm excitation/528 nm emission. The FITC-dextran concentration was normalized to body weight (mg/kg) by dividing the measured concentration ($\mu\text{g/mL}$) by the corresponding animal body mass (kg).

Tissue Sample Collection from Mice and Pathological Examination. After euthanasia by cervical dislocation, target tissues (liver, white adipose tissue (WAT), jejunum, ileum, and colon) were removed and fixed in 10% neutral buffered formalin for 48 h, processed for paraffin embedding, sectioned at 3 μm thickness, and stained with hematoxylin and eosin (H&E). Periodic acid–Schiff (PAS)/hematoxylin staining was performed for goblet cells. Light microscopy imaging and analysis were conducted utilizing the Leica DMR microscope system (Leica Microsystems, Wetzlar, Germany). Quantitative histological analysis was implemented under blinded conditions, with goblet cell counts normalized to villus architecture through pathologist-verified protocols. For each sample, 5–7 fields with at least ten complete contiguous crypts were analyzed. Images were analyzed using ImageJ.

Immunohistochemical Analysis. After deparaffinization and antigen retrieval (EDTA, pH 8.0), immunofluorescent detection of the tight junction protein Zonula occludens-1 (ZO-1) was performed with rabbit anti-ZO-1 polyclonal antibody (21773–1-AP, Proteintech, China) incubation at $4\text{ }^{\circ}\text{C}$ overnight, followed with Alexa Fluor 594-conjugated goat antirabbit IgG (H+L) (ZSGB-BIO, Beijing, China) incubation at $37\text{ }^{\circ}\text{C}$ for 1 h. After the coverslip was mounted with antifade mountant containing DAPI (ZSGB-BIO), the slides were observed and photographed under a Leica TCS SP8 laser confocal microscope with LAS X Life Science Microscope Software (USA).

RNA Exaction, Reverse Transcription, and Quantitative Real-Time PCR. The aliquots of intestinal samples were frozen in liquid nitrogen and maintained at $-80\text{ }^{\circ}\text{C}$. RNA was extracted with Trizol reagent (ThermoFisher Scientific, Shanghai, China), reverse transcription was performed utilizing PrimeScript RT Master Mix (Takara Biomedical Technology Co., Ltd., China), and quantification was carried out by real-time PCR with TB Green Premix Ex Taq (Takara) and an ABI

7500 (Applied Biosystems Inc., CA, USA). Gene expression quantification was performed via the comparative threshold cycle (delta-delta Ct method). Oligonucleotide primer sequences are detailed in Supplementary Table S1.

Statistical Analysis. All quantitative results are reported as mean \pm SD values. Intergroup comparisons were assessed using the *t*-test or Mann–Whitney U test. Multiple group comparisons were conducted through a one-way analysis of variance (ANOVA) with the least significant difference (LSD) or Kruskal–Wallis multicomparisons test on IBM SPSS software version 22.0. Significance was determined at $p < 0.05$.

■ ASSOCIATED CONTENT

SI Supporting Information

The Supporting Information is available free of charge at <https://pubs.acs.org/doi/10.1021/acsomega.5c01210>.

The Supporting Information contains: Supplementary Table 1: sequences of primers. Supplementary Figure 1: community assessment of gut microbiome in HIV-1 infectors receiving DTG-based and EFV-based combination antiretroviral therapy (cART). Supplementary Figure 2: oral glucose tolerance test (OGTT) in efavirenz (EFV)-treated and dolutegravir (DTG)-treated mice. Supplementary Figure 3: histopathologic changes in liver and adipose of efavirenz (EFV)-treated and dolutegravir (DTG)-treated mice. Supplementary Figure 4: suppressed expression of pyruvate metabolism-associated genes in the ileum caused by EFV versus DTG. Supplementary Figure 5: community assessment of gut microbiome in DTG and EFV treated mice. Supplementary Figure 6: genera with differential abundance and predicted Kyoto Encyclopedia of Genes and Genomes (KEGG) pathways enriched in EFV group compared to NC group. Supplementary Figure 7: genera with differential abundance and predicted Kyoto Encyclopedia of Genes and Genomes (KEGG) pathways enriched in DTG group compared to NC group (PDF)

■ AUTHOR INFORMATION

Corresponding Authors

Hai-Peng Zhu – Dongguan Ninth People's hospital, Dongguan 523001, China; Email: zhuhaipeng0616@sohu.com

Song Chen – Science and Technology Innovation Center, Guangzhou University of Chinese Medicine, Guangzhou 510405, China; orcid.org/0000-0003-2521-717X; Email: chensong@gzucm.edu.cn

Authors

Yong-Xiang Huang – Science and Technology Innovation Center, Guangzhou University of Chinese Medicine, Guangzhou 510405, China

Qin Tang – Science and Technology Innovation Center, Guangzhou University of Chinese Medicine, Guangzhou 510405, China; Jiangxi Provincial People's Hospital & The First Affiliated Hospital of Nanchang Medical College, Nanchang 330006, China

Shi-Hua Fu – Dongguan Ninth People's hospital, Dongguan 523001, China

Hui-Jun Zhong – Dongguan Ninth People's hospital, Dongguan 523001, China

Zhe Liu – Science and Technology Innovation Center, Guangzhou University of Chinese Medicine, Guangzhou 510405, China

Qing-Yang Zhong – Dongguan Ninth People's hospital, Dongguan 523001, China

Yan-Hao Wang – Dongguan Ninth People's hospital, Dongguan 523001, China

Yin-di Luo – Dongguan Ninth People's hospital, Dongguan 523001, China

Xue-Ying Li – Science and Technology Innovation Center, Guangzhou University of Chinese Medicine, Guangzhou 510405, China

Complete contact information is available at:

<https://pubs.acs.org/10.1021/acsomega.5c01210>

Author Contributions

#Y.X.H. and Q.T. have contributed equally to this work. Q.T. and Y.X.H.: data curation, formal analysis, writing—original draft. Z.L. and X.Y.L.: investigation and methodology. S.H.F., H.J.Z., Q.Y.Z., Y.H.W., and Y.D.L.: project administration, conceptualization, writing—review and editing; S.C. and H.P.Z. Conceptualization and funding acquisition: H.P.Z.

Funding

This work was supported by the project “Dongguan Science and Technology of Social Development Program” (Nos 2020507150119175 and 20221800905402) and the Key Research Laboratory and Key Discipline Development Project for Traditional Chinese Medicine in the Prevention and Treatment of Infectious Diseases, funded by the Traditional Chinese Medicine Bureau of Guangdong Province.

Notes

The authors declare no competing financial interest.

■ ACKNOWLEDGMENTS

We thank the Lingnan Medical Research Center of Guangzhou University of Chinese Medicine for providing some of the laboratory facilities used in this study.

■ ABBREVIATIONS

EFV, efavirenz; DTG, dolutegravir; cART, combination antiretroviral therapy; LPS, lipopolysaccharide; sCD14, soluble CD14; CI, confidence interval; TC, total cholesterol; LDL-c, low-density lipoprotein cholesterol; HDL-c, high-density lipoprotein cholesterol; TG, triglycerides; MPC1, mitochondrial pyruvate carrier 1; MPC2, mitochondrial pyruvate carrier 2; PDHA1, pyruvate dehydrogenase E1 subunit alpha 1; NDUFV1, NADH: ubiquinone oxidoreductase core subunit V1; NDUFV2, NADH: ubiquinone oxidoreductase core subunit V2; NDUFS1, NADH: ubiquinone oxidoreductase core subunit S1; SDHA, succinate dehydrogenase complex flavoprotein subunit A; GAPDH, glyceraldehyde 3-phosphate dehydrogenase

■ REFERENCES

- (1) Lochet, P.; Peyriere, H.; Lotthe, A.; Mauboussin, J. M.; Delmas, B.; Reynes, J. Long-term assessment of neuropsychiatric adverse reactions associated with efavirenz. *HIV Med.* **2003**, *4* (1), 62–66.
- (2) Haubrich, R. H.; Riddler, S. A.; DiRienzo, A. G.; Komarow, L.; Powderly, W. G.; Klingman, K.; Garren, K. W.; Butcher, D. L.; Rooney, J. F.; Haas, D. W.; et al. Metabolic outcomes in a randomized trial of nucleoside, nonnucleoside and protease inhibitor-sparing regimens for initial HIV treatment. *AIDS* **2009**, *23* (9), 1109–1118.

- (3) Phulara, N. R.; Rege, A.; Bieberich, C. J.; Seneviratne, H. K. Mass Spectrometry Imaging Reveals Region-Specific Lipid Alterations in the Mouse Brain in Response to Efavirenz Treatment. *ACS Pharmacol. Transl. Sci.* **2024**, *7* (8), 2379–2390.
- (4) Phulara, N. R.; Seneviratne, H. K. Visualization of Efavirenz-Induced Lipid Alterations in the Mouse Brain Using MALDI Mass Spectrometry Imaging. *Curr. Protoc.* **2025**, *5* (2), No. e70108.
- (5) Global HIV, Hepatitis and STIs Programmes (HHS), World Health Organisation. Updated recommendations on first-line and second-line antiretroviral regimens and post-exposure prophylaxis and recommendations on early infant diagnosis of HIV: interim guidelines. Supplement to the 2016 consolidated guidelines on the use of antiretroviral drugs for treating and preventing HIV infection; World Health Organisation: Geneva, 2018, (WHO/CDS/HIV/18.51).
- (6) Blanco, J. R.; Alejos, B.; Moreno, S. Impact of dolutegravir and efavirenz on immune recovery markers: Results from a randomized clinical trial. *Clin Microbiol Infect.* **2018**, *24* (8), 900–907.
- (7) Kronsten, V. T.; Tranah, T. H.; Pariente, C.; Shawcross, D. L. Gut-derived systemic inflammation as a driver of depression in chronic liver disease. *J. Hepatol.* **2022**, *76* (3), 665–680.
- (8) Mangiola, F.; Ianiro, G.; Franceschi, F.; Fagioli, S.; Gasbarrini, G.; Gasbarrini, A. Gut microbiota in autism and mood disorders. *World J. Gastroenterol.* **2016**, *22* (1), 361–368.
- (9) Anderson, G.; Seo, M.; Berk, M.; Carvalho, A. F.; Maes, M. Gut Permeability and Microbiota in Parkinson's Disease: Role of Depression, Tryptophan Catabolites, Oxidative and Nitrosative Stress and Melatonergic Pathways. *Curr. Pharm. Des.* **2016**, *22* (40), 6142–6151.
- (10) Thu Thuy Nguyen, V.; Endres, K. Targeting gut microbiota to alleviate neuroinflammation in Alzheimer's disease. *Adv. Drug Delivery Rev.* **2022**, *188*, 114418.
- (11) Ghazalpour, A.; Cespedes, I.; Bennett, B. J.; Allayee, H. Expanding role of gut microbiota in lipid metabolism. *Curr. Opin. Lipidol.* **2016**, *27* (2), 141–147.
- (12) Zhang, R.; Bao, J.; Qiao, J.; Li, W.; Qian, F.; Hu, K.; Sun, B. Long-term efavirenz exposure induced neuroinflammation and cognitive deficits in C57BL/6 mice. *Biochem. Biophys. Res. Commun.* **2021**, *584*, 46–52.
- (13) Jung, I.; Tu-Sekine, B.; Jin, S.; Anokye-Danso, F.; Ahima, R. S.; Brown, T. T.; Kim, S. F. Dolutegravir Suppresses Thermogenesis via Disrupting Uncoupling Protein 1 Expression and Mitochondrial Function in Brown/Beige Adipocytes in Preclinical Models. *J. Infect. Dis.* **2022**, *226* (9), 1626–1636.
- (14) Blas-Garcia, A.; Apostolova, N.; Ballesteros, D.; Monleon, D.; Morales, J. M.; Rocha, M.; Victor, V. M.; Esplugues, J. V. Inhibition of mitochondrial function by efavirenz increases lipid content in hepatic cells. *Hepatology* **2010**, *52* (1), 115–125.
- (15) Marchetti, G.; Tincati, C.; Silvestri, G. Microbial translocation in the pathogenesis of HIV infection and AIDS. *Clin. Microbiol. Rev.* **2013**, *26* (1), 2–18.
- (16) Trzeciak, P.; Herbet, M. Role of the Intestinal Microbiome, Intestinal Barrier and Psychobiotics in Depression. *Nutrients* **2021**, *13* (3), 927.
- (17) Ray, S.; Narayanan, A.; Giske, C. G.; Neogi, U.; Sonnerborg, A.; Nowak, P. Altered Gut Microbiome under Antiretroviral Therapy: Impact of Efavirenz and Zidovudine. *ACS Infect. Dis.* **2021**, *7* (5), 1104–1115.
- (18) McNaught, C. E.; Woodcock, N. P.; MacFie, J.; Mitchell, C. J. A prospective randomised study of the probiotic *Lactobacillus plantarum* 299V on indices of gut barrier function in elective surgical patients. *Gut* **2002**, *51* (6), 827–831.
- (19) Apostolova, N.; Gomez-Sucerquia, L. J.; Moran, A.; Alvarez, A.; Blas-Garcia, A.; Esplugues, J. V. Enhanced oxidative stress and increased mitochondrial mass during efavirenz-induced apoptosis in human hepatic cells. *Br. J. Pharmacol.* **2010**, *160* (8), 2069–2084.
- (20) Jung, I.; Tu-Sekine, B.; Jin, S.; Anokye-Danso, F.; Ahima, R. S.; Brown, T. T.; Kim, S. F. Dolutegravir Suppresses Thermogenesis via Disrupting UCP1 Expression and Mitochondrial Function in Brown/Beige Adipocytes in preclinical models. *J. Infect. Dis.* **2022**, *226* (9), 1626–1636.
- (21) Ajaykumar, A.; Caloren, L. C.; Povshedna, T.; Hsieh, A. Y. Y.; Zakaria, A.; Cai, R.; Smith, M. R.; Thompson, C. A. H.; Becquart, P.; Uday, P.; et al. Dolutegravir-containing HIV therapy reversibly alters mitochondrial health and morphology in cultured human fibroblasts and peripheral blood mononuclear cells. *AIDS* **2023**, *37* (1), 19–32.
- (22) Crakes, K. R.; Santos Rocha, C.; Grishina, I.; Hirao, L. A.; Napoli, E.; Gaulke, C. A.; Fenton, A.; Datta, S.; Arredondo, J.; Marco, M. L.; et al. PPARalpha-targeted mitochondrial bioenergetics mediate repair of intestinal barriers at the host-microbe intersection during SIV infection. *Proc. Natl. Acad. Sci. U. S. A.* **2019**, *116* (49), 24819–24829.
- (23) Schell, J. C.; Wisidagama, D. R.; Bensard, C.; Zhao, H.; Wei, P.; Tanner, J.; Flores, A.; Mohlman, J.; Sorensen, L. K.; Earl, C. S.; et al. Control of intestinal stem cell function and proliferation by mitochondrial pyruvate metabolism. *Nat. Cell Biol.* **2017**, *19* (9), 1027–1036.
- (24) Bricker, D. K.; Taylor, E. B.; Schell, J. C.; Orsak, T.; Boutron, A.; Chen, Y. C.; Cox, J. E.; Cardon, C. M.; Van Vranken, J. G.; Dephoure, N.; et al. A mitochondrial pyruvate carrier required for pyruvate uptake in yeast, *Drosophila*, and humans. *Science* **2012**, *337* (6090), 96–100.
- (25) Le Chatelier, E.; Nielsen, T.; Qin, J.; Prifti, E.; Hildebrand, F.; Falony, G.; Almeida, M.; Arumugam, M.; Batto, J. M.; Kennedy, S.; et al. Richness of human gut microbiome correlates with metabolic markers. *Nature* **2013**, *500* (7464), 541–546.
- (26) Zhu, Y.; Chen, B.; Zhang, X.; Akbar, M. T.; Wu, T.; Zhang, Y.; Zhi, L.; Shen, Q. Exploration of the Muribaculaceae Family in the Gut Microbiota: Diversity, Metabolism, and Function. *Nutrients* **2024**, *16* (16), 2660.
- (27) Kenedi, C. A.; Goforth, H. W. A systematic review of the psychiatric side-effects of efavirenz. *Aids Behav.* **2011**, *15* (8), 1803–1818.
- (28) Lagod, P. P.; Naser, S. A. The Role of Short-Chain Fatty Acids and Altered Microbiota Composition in Autism Spectrum Disorder: A Comprehensive Literature Review. *Int. J. Mol. Sci.* **2023**, *24* (24), 17432.
- (29) Li, H.; Guo, W.; Li, S.; Sun, B.; Li, N.; Xie, D.; Dong, Z.; Luo, D.; Chen, W.; Fu, W.; et al. Alteration of the gut microbiota profile in children with autism spectrum disorder in China. *Front. Microbiol.* **2024**, *14*, 1326870.
- (30) Radjabzadeh, D.; Bosch, J. A.; Uitterlinden, A. G.; Zwinderman, A. H.; Ikram, M. A.; van Meurs, J. B. J.; Luik, A. I.; Nieuwdorp, M.; Lok, A.; van Duijn, C. M.; et al. Gut microbiome-wide association study of depressive symptoms. *Nat. Commun.* **2022**, *13* (1), 7128.
- (31) Branton, W. G.; Ellestad, K. K.; Maingat, F.; Wheatley, B. M.; Rud, E.; Warren, R. L.; Holt, R. A.; Surette, M. G.; Power, C. Brain microbial populations in HIV/AIDS: Alpha-proteobacteria predominate independent of host immune status. *PLoS One* **2013**, *8* (1), No. e54673.
- (32) Salonen, A.; Nikkila, J.; Jalanka-Tuovinen, J.; Immonen, O.; Rajilic-Stojanovic, M.; Kekkonen, R. A.; Palva, A.; de Vos, W. M. Comparative analysis of fecal DNA extraction methods with phylogenetic microarray: Effective recovery of bacterial and archaeal DNA using mechanical cell lysis. *J. Microbiol. Methods.* **2010**, *81* (2), 127–134.
- (33) Kozich, J. J.; Westcott, S. L.; Baxter, N. T.; Highlander, S. K.; Schloss, P. D. Development of a dual-index sequencing strategy and curation pipeline for analyzing amplicon sequence data on the MiSeq Illumina sequencing platform. *Appl. Environ. Microbiol.* **2013**, *79* (17), 5112–5120.
- (34) Langille, M. G.; Zaneveld, J.; Caporaso, J. G.; McDonald, D.; Knights, D.; Reyes, J. A.; Clemente, J. C.; Burkpile, D. E.; Vega Thurber, R. L.; Knight, R.; et al. Predictive functional profiling of microbial communities using 16S rRNA marker gene sequences. *Nat. Biotechnol.* **2013**, *31* (9), 814–821.

(35) Guide for the Care and Use of Laboratory Animals 8th National Academies Collection: Reports Funded By National Institutes Of Health; National Academies Press: Washington (DC) 2011